CuNi Dendritic Material: Synthesis, Mechanism Discussion, and Application as Glucose Sensor

Ri Qiu, Xiao Li Zhang, Ru Qiao, Yan Li, Yeong Il Kim, and Young Soo Kang*

Department of Chemistry, Pukyong National University, 599-1 Daeyeon-3-dong, Namgu, Busan, 608-737, Korea

Received March 7, 2007. Revised Manuscript Received June 12, 2007

CuNi dendritic material has been obtained by the electrochemical method. For the synthesis of the material, different potentials were applied to get the dendritic structure in the aqueous solution. The materials were characterized by a series of techniques. The morphology of the material was characterized by field-emission scanning electron microscopy and high-resolution transmission electron microscopy. Energy-dispersive spectroscopy was applied to analyze the elemental composition. X-ray diffraction was used to check the crystal structure of the deposit. The dendritic morphology formation mechanism is discussed from the aspects of thermodynamics and kinetics to give a deep understanding of the crystal growth. For the potential practical application of the material in the fuel cell and biosensor, the electrooxidation ability of glucose in alkaline solution was tested, and the sensor based on this dendritic alloy was tried.

Introduction

CuNi material is a kind of catalyst widely used in many fields, e.g., methanol synthesis from a mixture of hydrogen and carbon dioxide (or carbon monoxide);[1] dehydrogenation reaction from alcohol to get hydrogen for the application in the fuel cell.[2−12] In the electrochemical fields, CuNi material is one of versatile alloys that can be applied to the catalyst of electrochemical processes to realize the small molecule (H_2, methanol, glucose, nitroalkane, nitrate, and nitrite etc.) transformations, which are important issues for fuel cell (H_2, methanol), biosensor (glucose), and even environmental problems (nitroalkane, nitrate, and nitrite, etc.). Much attention has been paid to the electrocatalytic applications in these fields.[13−14]

A dendrite is a kind of material that has a main stem from which many side branches grow out. The term of "dendrite" comes from the Greek word "dendron" with the meaning of "tree". The dendrite has a hierarchical structure with primary, secondary, tertiary, and even higher-order branches.[15] Many reports about the dendritic material synthesis have been found until now because of its potential application to the catalysis and technological fields. Dendrite nanostructures can be fabricated by metals (including noble and transition metals),[16−27] metal oxides,[28,29] and semicoductors.[30] Up to now, the methods to get the dendritic material are mainly based on the solvothermal method, hydrothermal method, solution-phase synthesis, and the chemical vapor deposition method.

* Corresponding author. E-mail: yskang@pknu.ac.kr.

(1) Nerlov, J.; Chorkendorff, I. *J. Catal.* **1999**, *181*, 271.
(2) Fatsikostas, A. N.; Kondarides D. I.; Verykios, X. E. *Chem. Commun.* **2001**, 851.
(3) Fatsikostas, A. N.; Kondarides, D. I.; Verykios, X. E. *Catal. Today* **2002**, *75*, 145.
(4) Fatsikostas, A. N.; Verykios, X. E. *J. Catal.* **2004**, *225*, 439.
(5) Frusteri, F.; Freni, S.; Chiodo, V.; Spadaro, L.; Di Blasi, O.; Bonura, G.; Cavallaro, S. *Appl. Catal., A* **2004**, *270*, 1.
(6) Breen, J.; Burch, P. R.; Coleman, H. M. *Appl. Catal., B* **2002**, *39*, 65.
(7) Aupretre, F.; Descorme, C.; Duprez, D. *Catal. Commun.* **2002**, *3*, 267.
(8) Freni, S.; Cavallaro, S.; Mondello, N.; Spadaro, L.; Frusteri, F. *Catal. Commun.* **2003**, *4*, 259.
(9) Frusteri, F.; Freni, S.; Spadaro, L.; Chiodo, V.; Bonura, G.; Donato, S.; Cavallaro, S. *Catal. Commun.* **2004**, *5*, 611.
(10) Fierro, V.; Klouz, V.; Akdim, O.; Mirodatos, C. *Catal. Today* **2002**, *75*, 141.
(11) Marino, F.; Baronetti, G.; Jobbagy, M.; Laborde, M. *Appl. Catal. A: Gen.* **2003**, *238*, 41.
(12) Zhang, Z.; Verykios, X. E. *Chem. Commun.* **1995**, 71.
(13) Sinfelt, John H. *Bimetallic Catalysts: Discoveries, Concepts, and Applications*; John Wiley & Sons: New York, 1983.
(14) Lipkowski, J.; Ross, P. N. *Electrocatalysis*; Wiley-VCH: Weinheim, Germany, 1998.
(15) Galenko, P. K.; Zhuravlev, V. A. *Physics of Dendrites: Computational Experiments*; World Scientific: Singapore, 1994.
(16) Hao, E.; Bailey, R. C.; Schatz, G. C.; Hupp, J. T.; Li, S. Y. *Nano Lett.* **2004**, *4*, 327.
(17) Chen, S. H.; Wang, Z. L.; Ballato, J.; Foulger, S. H.; Carroll, D. L. *J. Am. Chem. Soc.* **2003**, *125*, 16186.
(18) Herricks, T.; Chen, J. Y.; Xia, Y. N. *Nano Lett.* **2004**, *4*, 2367.
(19) Teng, X. W.; Yang, H. *Nano Lett.* **2005**, *5*, 885.
(20) Ramirez, E.; Jansat, S.; Philippot, K.; Lecante, P.; Gomez, M.; Masdeu-Bulto, A. M.; Chaudret, B. *J. Organomet.Chem.* **2004**, *689*, 4601.
(21) Antonietti, M.; Goltner, C. *Angew. Chem., Int. Ed.* **1997**, *36*, 910.
(22) Ewers, T. D.; Sra, A. K.; Norris, B. C.; Cable, R. E.; Cheng, C. H.; Shantz, D. F.; Schaak, R. E. *Chem. Mater.* **2005**, *17*, 514.
(23) Hoefelmeyer, J. D.; Niesz, K.; Somorjai, G. A.; Tilley, T. D. *Nano Lett.* **2005**, *5*, 435.
(24) Ould-Ely, T.; Amiens, C.; Chaudret, B.; Snoeck, E.; Verelst, M.; Respaud, M.; Broto, J. M. *Chem. Mater.* **1999**, *11*, 526.
(25) Vidoni, O.; Philippot, K.; Amiens, C.; Chaudret, B.; Balmes, O.; Malm, J. O.; Bovin, J. O.; Senocq, F.; Casanove, M. J. *Angew. Chem., Int. Ed.* **1999**, *38*, 3736.
(26) Pelzer, K.; Vidoni, O.; Philippot, K.; Chaudret, B.; Colliere, V. *Adv. Funct. Mater.* **2003**, *13*, 118.
(27) Wen, X.; Xie, Y.-T.; Mak, W. C.; Cheung, K. Y.; Li, X.-Y.; Renneberg, R.; Yang, S. *Langmuir* **2006**, *22*, 4836.
(28) Yan, H.; He, R.; Johnson, J.; Law, M.; Saykally, R. J.; Yang, P. *J. Am. Chem. Soc.* **2003**, *125*, 4728.
(29) Cao, M.; Liu, T.; Gao, S.; Sun, G.; Wu, X.; Hu, C.; Wang, Z. L. *Angew. Chem.* **2005**, *117*, 4269. *Angew. Chem., Int. Ed.* **2005**, *44*, 4197.
(30) Kanaras, A. G.; Sönnichsen, C.; Liu, H.; Alivisatos, A. P. *Nano Lett.* **2005**, *5*, 2164.

10.1021/cm070638a CCC: $37.00
Published on Web 07/21/2007

It has been a long history for dendritic structure formation from the electrolysis.[31] These years, much attention has been paid to dendritic nanomaterial fabrication on the basis of the electrochemical methods.[32−34] If the dendritic structure can be electrodeposited on the surface of the electrode, the modified electrode with a high surface area can be used as the electrochemical devices in the fields of fuel cells, sensors, and batteries. The open porous structure will be critical for the mass transfer, which is important in the electrochemical reaction. For the dendritic material, there are few reports considering the practical application.[27] The further research for dendritic material applications is to be deserved.

The current methods to get CuNi or Ni material are mainly based on the electroplating and solution reduction methods.[35−37] Herein, we show the electrochemical method to get CuNi dendritic material. There have been reports about this alloy material synthesis via the electrodeposition methods.[38−41] We have made detailed discussion to the dendritic material formation mechanism from the thermodynamics and kinetics perspectives. For its potential practical application, the as-obtained dendritic material was checked by the voltammetric technique to see its electrooxidation ability to the glucose, which is of great importance for the construction of glucose sensor and fuel cell. The sugar sensors based on the copper and nickel materials have been reported previously.[42−44] In our research, we show that the electrode modified by CuNi dendritic material is the potential glucose sensor. For the strategy we take to manage the sensor, there are several outstanding merits: (1) For the electrocatalysis, we applied the dendrite-modified electrode to the electrocatalysis directly, and there is no need for other instruments to assemble the electrode. (2) This kind of sensor for the glucose detection is enzyme-free and will be more convenient than the traditional enzymic sensors.[43] (3) The CuNi composition in the deposit can be controlled by the applied potential during the electrolysis process directly. The general relationship between the CuNi composition and electrocatalysis ability is available. (4) The research is not only important for glucose detection, which is of considerable significance in many areas such as clinical diagnostics and biotechnology, but also of further importance in the sugar fuel-cell field.

(31) Matsushita, M.; Sano, M.; Hayakawa, Y.; Honjo, H.; Sawada, Y. *Phys. Rev. Lett.* **1984**, *53*, 286.
(32) Shin, H.; Dong, J.; Liu, M. *Adv. Mater*. **2003**, *15*, 1610.
(33) Lopez, Carmen M.; Choi, K. S. *Langmuir* **2006**, *22*, 10625.
(34) Panda, B. R.; Rao, P. N.; Paul, A.; Chattopadhyay, A. *J. Phys. Chem. B* **2006**, *110*, 22917.
(35) Delatorre, R. G.; Sartorelli, M. L.; Schervenski, A. Q.; Pasa, A. A. *J. Appl. Phys.* **2003**, *93*, 6154.
(36) Sun, L.; Chien, C. L.; Searson, Peter C. *Chem. Mater.* **2004**, *16*, 3125.
(37) Zhang, X.; Tu, K. N. *J. Am. Chem. Soc*. **2006**, *128*, 15036.
(38) Kazeminezhad, I.; Blythe, H. J.; Schwarzacher, W. *Appl. Phys. Lett.* **2001**, *78*, 1014.
(39) Jović. V. D.; Jović, B. M.; Pavlović, M. G. *Electrochim. Acta* **2006**, *51*, 5468.
(40) Kupper, M.; Schultze, J. W. *Electrochim. Acta* **1997**, *42*, 3023.
(41) Baskaran, I.; Sankara Narayanan, T. S. N.; Stephen, A. *Mater. Lett.* **2006**, *60*, 1990.
(42) You, T.; Niwa, O.; Chen, Z.; Hayashi, K.; Tomita, M.; Hirono, S. *Anal. Chem.* **2003**, *75*, 5191.
(43) Park, S.; Boo, H.; Chung, T. D. *Anal. Chim. Acta* **2006**, *556*, 46.
(44) Lawrence, N. S.; Beckett, E. L.; Davis, J.; Compton, R. G. *Anal. Biochem.* **2002**, *303*, 1.

Experimental Section

Preparation and Characterization of CuNi Dendritic Structure. A typical electrolysis process was conducted as follows: The synthesis of CuNi dendritic material was performed in a simple three-electrode cell by using an EG&G potentiostat/galvanostat M263 A instrument. High-purity Cu foil (Aldrich, 99.98%, 0.5 mm thick), scratched by sand paper, cleaned with deionized water (>18 MΩ cm, Nanopure Ultrapure water system), was used as the substrate for CuNi electrodeposition. The area of the electrode dipped into the solution was fixed to be 0.4 cm^2. Coiled Pt wire electrode was applied as the counter electrode, and saturated calomel electrode (SCE) as the reference electrode. The distance between working and counter electrode was about 2.0 cm. The tip of the reference electrode was in the vicinity of the working electrode. A 15 mL mixed solution containing 0.03 M $NiSO_4$(Aldrich, 99%), 0.03 M $CuCl_2$ (Aldrich, 99+%), and 0.1 M Na_2SO_4 (Shinyo Pure Chemicals, G.R. reagent) was added into the cell to be electrolyzed.

Chronoamperometry technique was applied to electrolyze the mixed solution, and different potentials, e.g., −0.8, −1.0, −1.2 V, (vs SCE), were applied to get the deposit. Electrodeposition process was performed in a stationary electrolyte solution without any stirring or protective gas bubbling. After electrolysis, the electrode was brought out and washed by deionized water and acetone several times to get rid of the impurities.

The morphology of the materials obtained with different potentials were characterized by field-emission scanning electron microscope (FE-SEM, JEOL, JSM-6700F), and high-resolution transmission electron microscope (HRTEM, JEOL. JEM-2010). Energy-dispersive spectroscopy (EDS, Oxford Instruments, INCA x-sight) was applied to analyze the elemental composition in the as-obtained material. X-ray diffraction (XRD, PHILIPS, X'Pert-MPD System, the X-ray is Cu Kα radiation with $\lambda = 0.154056$ nm.) was used to check the crystal structure of the deposition. For the EDS and XRD chracterization, the deposits were scratched off from the copper electrode to avoid the substrate influence.

Electrochemical Properties of CuNi Dendritic Material. The bare copper electrode and the copper electrodes modified by CuNi dendritic material were tested by the cyclic voltammetric (CV) technique to show the electro-oxidation ability of the glucose. The electrodes modified with CuNi dendritic material were obtained at the different potentials of −0.6, −0.8, −1.0, and −1.2 V (vs. SCE) with electrolysis time of 600 s. The area of the electrode dipped into the solution was fixed to be 0.4 cm^2. After the electrolysis, the electrode was moved out from the aqueous solution and washed by the deionized water. The electrode was put into the three-electrode cell to characterize its electrochemical properties. Coiled Pt wire electrode and SCE were applied as the counter electrode and reference electrode, respectively. The tip of the reference electrode was in the vicinity of the working electrode. A 10 mL aqueous solution containing 0.10 M NaOH (Shinyo Pure Chemicals, G.R.) was added into the cell for the blank CV test. After that process, the electrode was moved out and washed by deionized water to clean the electrode surface. Later, the electrode was put into a 10 mL mixed solution containing 0.10 M NaOH and 1.0 mM glucose (Katayama, First Class) to check the electrooxidation ability to the glucose. The CV scanning range was set to be 0−0.7 V (vs.SCE) with the rate of 50 mV/ s.

Electrochemical Measurement of CuNi Dendritic Material as Biosensor. Cu foil electrode modified by CuNi dendrites was obtained by the electrolysis at the potentials of −0.6 and −1.0 V (vs SCE) for 600 s. The area of the electrode dipped into the solution is 0.4 cm^2. After washing, the electrode was put into a 20 mL aqueous solution containing 0.10 M NaOH as the electrolyte. In the three-electrode system, coiled Pt wire electrode and SCE were

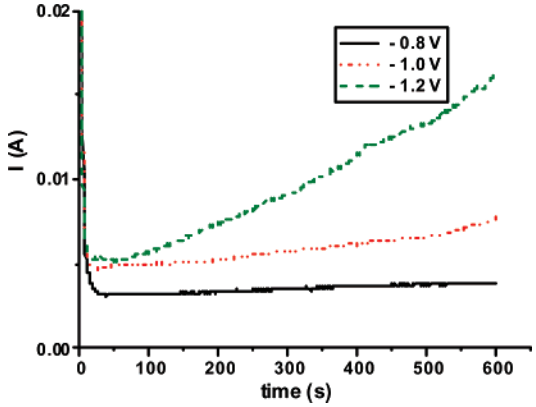

Figure 1. $I-t$ curves of the different potentials of −0.8, −1.0, and −1.2 V (vs SCE) with an electrolysis time of 600 s.

Table 1. Different Amounts of Mixed Solution Containing NaOH (0.1 M) and Glucose (1 mM) Added into the Cell at the Certain Electrolysis Times

no.	time solution added (s)	amount of solution added (mL)	[glucose] in cell (M)
1	150	0.04	2.0×10^{-6}
2	300	0.16	1.0×10^{-5}
3	450	0.80	4.8×10^{-5}
4	600	1.0	9.1×10^{-5}
5	800	9.0	3.5×10^{-4}

applied as the counter electrode and reference electrode, respectively. The chronoamperometry technique was applied to electrolyze the solution. The potential was set to be 0.65 V (vs.SCE), and the electrolysis time was 1200 s. The different volumes of mixed solution containing NaOH (0.1 M) and glucose (1 mM) were added into the cell with certain time intervals (Table 1) to show the electrode response to the different glucose concentrations.

Results and Discussion

Figure 1 shows the $I-t$ curves with the different electrolysis potentials. From the curves, it is obvious that the more negative potential will result in the larger reduction current. During the electrolysis process, the reactions of $Cu^{2+} + 2e^- = Cu$ (E^o= 0.339 V) and $Ni^{2+} + 2e^- = Ni$ (E^o= −0.236V, vs SHE) will happen on the working electrode.

The dendritic materials shown in Figures 2 and 3 were obtained at the potentials of −0.8 and −1.2 V with an electrolysis time of 3600 s. Although different potentials were applied during the electrolysis processes, the morphology of each is very similar. It is obvious that the deposit on the surface of the electrode was far from the flat film structure, and the dendritic structure was formed during the electroreduction process. The structure hierarchy and tip-splitting can be distinguished clearly, which can be found in images b and c of Figure 2 and Figure 3a. We assume that the tip-splitting in the branch tips and branch sides plays an important role during the dendrite growth. With the tip-splitting, the several ordered hierarchy structure will be realized.

The EDS of the material obtained at the potential of −0.8 V with electrolysis time of 3600 s is shown in Figure 2d. It is revealed that the as-obtained material is composed by copper and nickel elements. For the materials obtained at the different potentials, the atomic ratio between Ni and Cu will show the difference correspondingly. We applied EDS

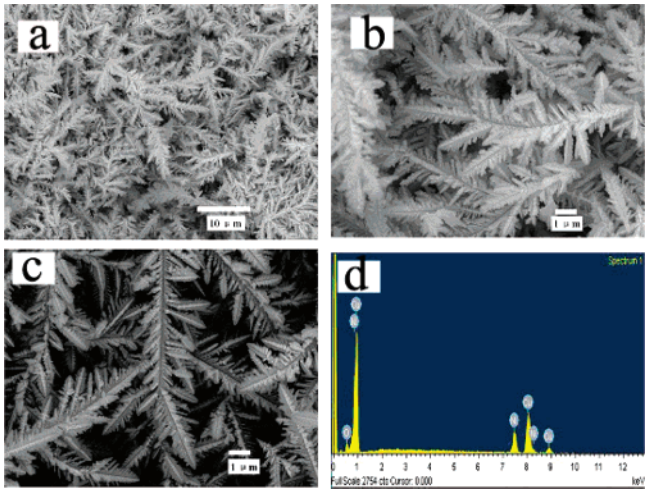

Figure 2. (a−c) FE-SEM images on the morphology of the CuNi dendritic materials obtained at a potential of −0.8 V with an electrolysis time of 3600 s. (d) Energy-dispersive X-ray spectrum of the as-obtained CuNi material.

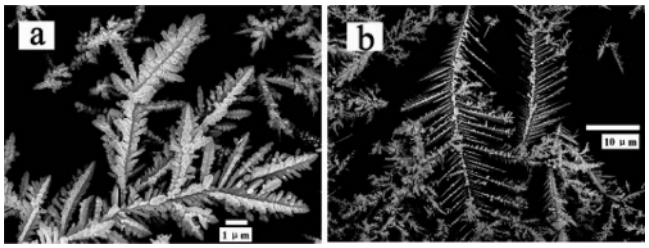

Figure 3. FE-SEM images on the morphology of CuNi dendritic material obtained at the potential of −1.2 V with an electrolysis time of 3600 s and different magnitudes.

Table 2. Atomic Ratio between Ni and Cu with the Different Electrolysis Potentials

	electrolysis time (s)	potential (V)	Cu:Ni
1	3600	−0.8	58.55:32.54
2	3600	−1.0	42.17:41.36
3	3600	−1.2	40.23:48.81

to get the Cu:Ni atomic ratio after the deposits were scratched off from the electrode. Table 2 lists the atomic ratio of the dendritic materials obtained at the different potentials with the same electrolysis time. It is obvious that the more negative potential is, the smaller the Cu:Ni ratio value will be.

For the understanding of elemental distribution in a dendrite, the material obtained at the potential of −1.0 V (vs SCE) with the electrolysis time of 2400 s was used for the analysis. We applied EDS to analyze the composition in different points along the direction of dendrite stem and branch. One of the dendrites was selected to check the Cu:Ni composition with five points. Shown in Figure 4, from points 1−5, the Cu:Ni ratios were 1.85, 2.97, 3.52, 1.82, and 4.00. It is proposed that the Cu:Ni ratio increases along the elongation direction of the stem in the dendrite. For the Cu/Ni ratio transition from point 1 to 4, it is not monotonous. The ratio value of point 1 is larger than that of point 4. This is attributed to the side-branching effect. The side branching can result in the abrupt crystal structure and even the elemental composition.[27] For the points 1−3, the regular monotonous change of atomic ratio can be observed. We ascribe it to two main reasons: (1) the difference between

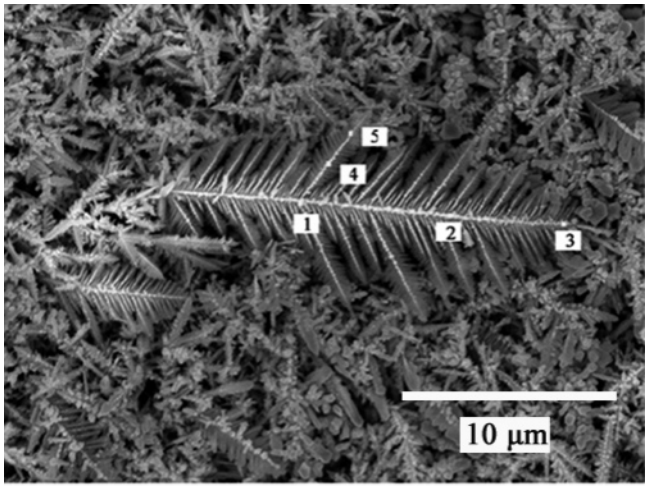

Figure 4. FE-SEM image of CuNi dendrites obtained at the potential of −1.0 V (vs SCE) with an electrolysis time of 2400 s. One CuNi dendrite was selected to check the Cu/Ni composition with the different points 1−5.

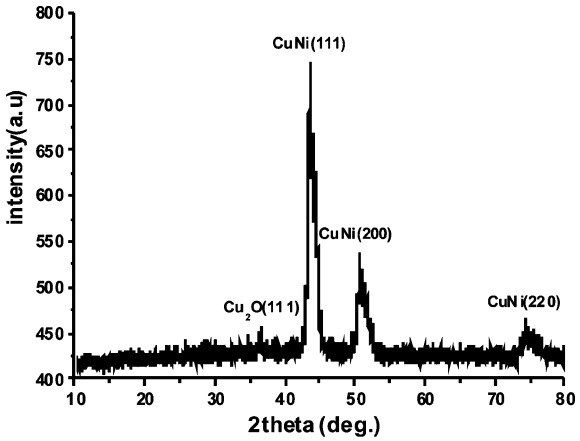

Figure 5. XRD pattern of the CuNi dendritic material obtained at the potential of −1.0 V (vs SCE) with an electrolysis time of 2400 s.

Table 3. Lattice Constants of Pure Copper and Different CuNi Alloy Phases Obtained from the JCPDS Cards and Unitcell Calculation

	lattice constant ($\times 10^{-10}$ m) (value from JCPDS)	lattice constant ($\times 10^{-10}$ m) (calculated value)	JCPDS no.
pure copper	3.6150	3.61492	04-0836
$Cu_{0.81}Ni_{0.19}$	3.5934	3.59292	47-1406
$Cu_{0.79}Ni_{0.21}$	3.595	3.59450	09-0205
dendritic CuNi		3.60113	

the diffusion ability between Cu^{2+} and Ni^{2+}, and (2) for the technique applied during the dendritic material formation, the potential of the working electrode is constant. With the electrolysis process going on, the length of the conductor will increase, and the resistance will become larger. The tip potential will be reduced to the less negative value, and the deposit will be Cu-rich.

To characterize the crystal structure, we also checked the same material by XRD and HRTEM. From the XRD pattern shown in Figure 5, the CuNi alloy phase is very distinguishable, although there is a Cu_2O peak due to the oxidation of the copper.

For the atomic composition of Cu and Ni in the alloy, it is suggested that there is a linear relationship between Cu elemental composition and lattice constant.[13] The Unitcell program was applied to calculate the lattice constant with the different Cu compositions to determine the lattice constant. From the data listed in Table 3, it is reliable to obtain the lattice constant with the software. The lattice constant value of the as-obtained CuNi material is between that for the pure Cu and $Cu_{0.81}Ni_{0.19}$. It is reasonable to confirm that the CuNi alloy phase is formed during the electrolysis process. The single-crystal structure was revealed by the electron diffraction (ED) shown in Figure 6.

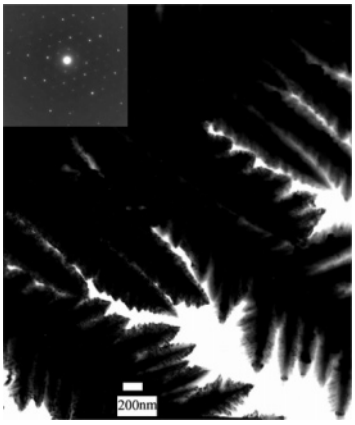

Figure 6. HRTEM and ED of the CuNi dendrite obtained at the potential −1.0 V with an electrolysis time of 2400 s.

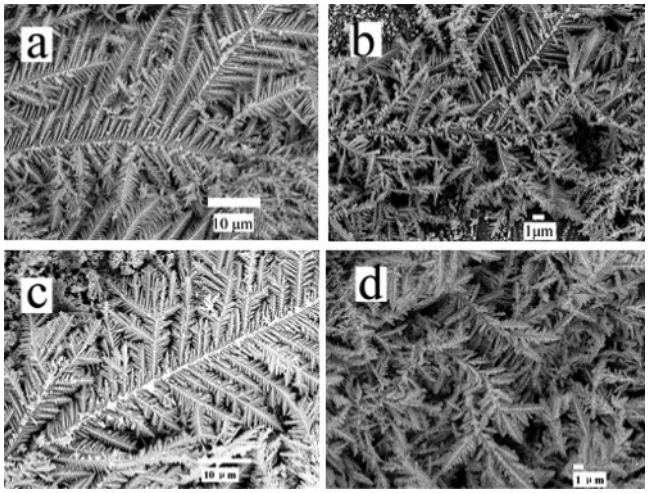

Figure 7. FE-SEM images of CuNi dendritic structures obtained at a potential of −1.0 V with different electrolysis times: (a) 60, (b) 300, (c) 600, and (d) 3600 s.

For the mechanism discussion, the electrolysis experiments based on the different potential and electrolysis time were tried to see the morphology difference. The dendritic structures obtained at the potential of −1.0 V with different electrolysis time are shown in Figure 7. It is observed that the morphology difference among the different electrolysis times is not very distinguishable. The dendrites of micrometer scale can be observed obviously. The morphologies obtained at the potential of −1.2 V (vs SCE) with different electrodeposition times are shown in Figure 8. From the images shown in Figure 8, the morphology of the material is not as exquisite as that of Figure 7, especially the short time depositions, e.g., 60 and 300 s. The structure obtained at −1.2 V with 60 s is very disordered (Figure 8a), and there is a peculiar dendritic stucture to be distinguished. For the longer electrolysis time, the dendrites can be found (Figure 8b−d). The materials obtained at −1.2 V with electrolysis

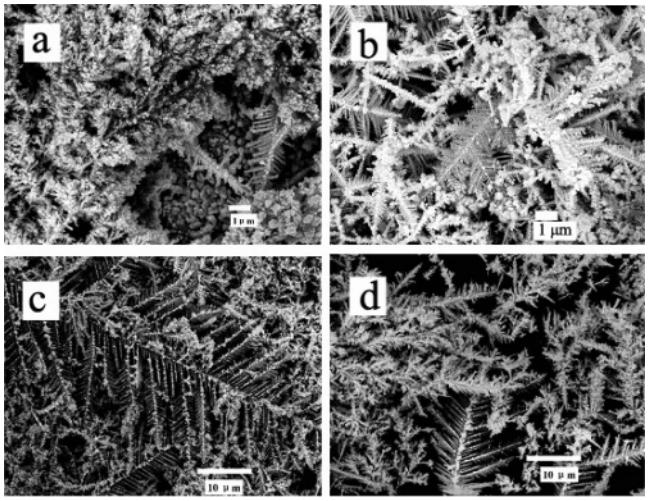

Figure 8. FE-SEM images of CuNi dendritic structures obtained at a potential of −1.2 V with different electrolysis times: (a) 60, (b) 300, (c) 600, and (d) 3600 s.

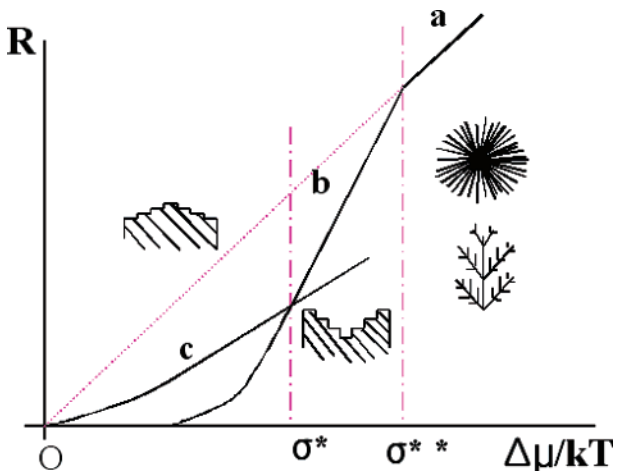

Figure 9. Schematic illustration between the solution supersaturation ($\Delta\mu/kT$) and growth rate (R) of the crystal growth from the solution phase.[45]

times of 60 and 300 s seem to be more random than the material obtained at −1.0 V with the same electrolysis time. If the electrolysis time is long enough, the morphology of the material obtained with the different potentials will be similar.

For the dendritic material formation mechanism based on the thermodynamics, we introduce the diagram between the supersaturation $\Delta\mu/kT$ and growth rate to explain the morphology variation with the different potentials applied during the same electrolysis time. The diagram shown as Figure 9 is originally described in the previous report[45] to give the consideration of the crystal growth from the solution phase. The driving force for the crystal growth is the supersaturation $\Delta\mu/kT$, in which $\Delta\mu$ is the chemical potential of the crystal growth, and k and T are the Boltzmann constant and temperature, respectively. From Figure 9, it is obvious that the crystal growth rate will be increased dramatically with the increase in supersaturation. With the change in the growth rate, the crystal will alter its external morphology to adapt the incoming mass transfer. Figure 9 shows the various morphologies obtained at the different supersaturation. With

(45) Sunagawa, I. *Morphology of Crystals;* Kluwer Academic: Dordrecht, The Netherlands, 1987.

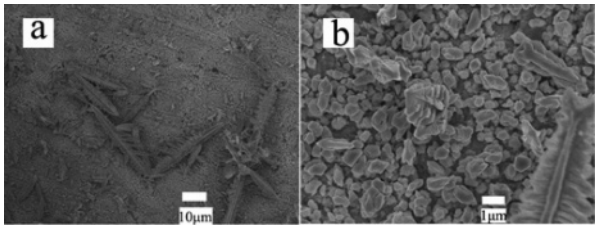

Figure 10. FE-SEM images of CuNi dendritic material obtained at the potential of −0.4 V with an electrolysis time of 600 s with magnitudes of 1000 and 9500.

the increase in supersaturation, the morphology will be changed from the convex surface to the concave hollow and even dendritic structure. For the experiments with electrochemical methods to fabricate the material, the potential applied to the working elecrode has a direct relationship to the Gibbs free energy, which is expressed as $\Delta G = -nFE$. The relationship between the supersaturation $\Delta\mu/kT$ and the potential is linear. The more negative a potential is, the larger the supersaturation of the reduced copper and nickel on the surface of the electrode will be. The crystal growth rate will be large enough for the morphology to take the dendritic form and even the disordered structure. From Figures 7a and 8a, the materials were obtained with the same growth time, but the more negative potential will result in the more disordered morphology. With the electrolysis process going on, the electric resistance of the electrode surface will be increased, the effective potential will be decreased, and the morphology of the materials obtained at −1.0 and −1.2 V will be similar.

For the kinetics mechanism discussion, we expect the growth mechanism can be revealed by the FE-SEM images from the as-obtained CuNi material. The material should be essentially stable to the water and oxygen during the preparation and treatment processes. In the CuNi alloy, the copper is more stable than nickel, which can be predicted from the standard reduction potentials ($Cu^{2+} + 2e^- = Cu$, $E^o = 0.339$ V; $Ni^{2+} + 2e^- = Ni$, $E^o = -0.236$V, vs SHE). From our experiments, we also discovered that the nickel-rich deposit obtained at the more negative potential will turn a green color easily becauss of the formation of nickel compounds. In contrast, the copper-rich material will be inert to the water and oxygen. The copper-rich material is appropriate in the mechanism discussion.

Electrolysis was taken at a potential of −0.4 V. After electrolysis for 600 s, the electrode was brought out of the solution to be washed and checked by the FE-SEM. We call it a quenching process. It is shown in Figure 10 that the crystals on the surface of the electrode are not uniform. When the growth was quenched, the scale distribution of the crystals was from several hundered nanometers to about 100 μm, because the nucleation and growth processes will not occur at the same time on the different sites of the electrode. The quenched crystals on different sites constitute a group, and the different morphology of the discrete crystals in the group can combine an integrated consecutive growth process of one single crystal from several hundred nanometers to nearly 100 μm.

Dendrite is a kind of crystal structure obtianed when the material scale reaches a certain degree. From the FE-SEM

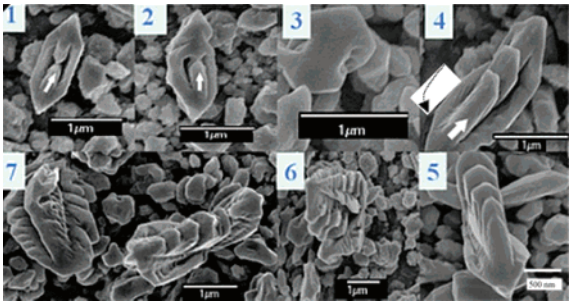

Figure 11. FE-SEM images of CuNi material shown as 1−7 are from the material obtained at a potential of −0.4 V with an electrolysis time of 600 s. Here is the schematic illustration of the growth evolution from defective crystal to the dendritic structure.

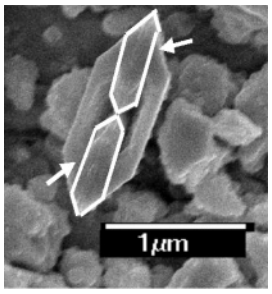

Figure 12. Hexagonal surfaces were formed during the crystal growth. The crystal will grow with consecutive mass transfer.

Table 4. Mass of the CuNi Obtained with Different Electrodeposition Potentials

electrolysis potential (V)	−0.6	−0.8	−1.0	−1.2
mass of deposit ($\times 10^{-4}$ g)	7.8	12.4	12.3	39.5

images shown in Figure 11, there is no distinguishable dendritic morphology with the scale below 1 μm. The submicrometer crystals are the embryos of the dendrites. The defects on the polyhedron surfaces cannot be avoided due to nonuniformity of mass transfer to the different directions of the crystal surfaces. With the crystal growth process going on, the primary effect caused by the defect will be magnified instead of being eliminated. It will play a key role to the distortion of the polyhedron. We select different crystals with defects to presume a representative growth mechanism. The growth evolution from defective crystal to the dendritic structure is schematically illustrated in Figure 11. The hexagonal crystal with two concave hollows is a very interesting morphology obtained on the electrode surface. We ascribe this to the flux nonuniformity among the different growth sites on the crystal growth. The growth rate on the suface edge is much faster than the inner sites. As the protrusion is formed on the edge, it will be even easier to get the mass transfer to support the further growth; meanwhile, the mass tranfer to the inner surface will decrease much more. This kind of location discrimination will be larger during the crystal growth instead of being surppressed. From Figure 11 (1) and Figure 12, we can see the hexagonal shape is formed on the surface of the crystal. We assume that hexagonal geometry is advantageous to the further crystal growth. With such geometry, the layer-by-layer spiral crystal growth will occur, and the growth competition between the two hexagonal surfaces will happen during the process. The results will be as follows: (1) One of them will grow faster, and the other will be hindered for the opportunity of growth

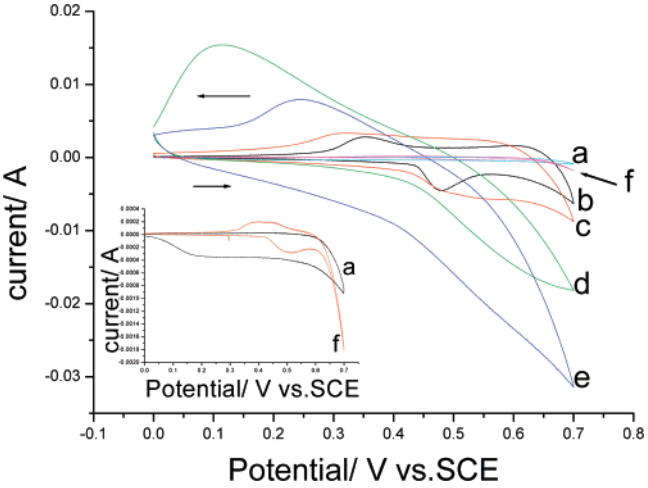

Figure 13. Cyclic voltammograms of the CuNi catalysts and copper foil in a 0.1 M NaOH aqueous solution with a scan rate of 50 mV/s. CuNi catalysts were deposited at different potentials, and the electrolysis times were all 600 s. (a) Copper foil, (f) nickel foil, (b−e) CuNi alloy obtained with different potentials: (b) −0.6, (c) −0.8, (d) −1.0, and (e) −1.2 V. To see the CV curves of (a) copper foil and (f) nickel foil clearly, the inset shows the comparison between the two.

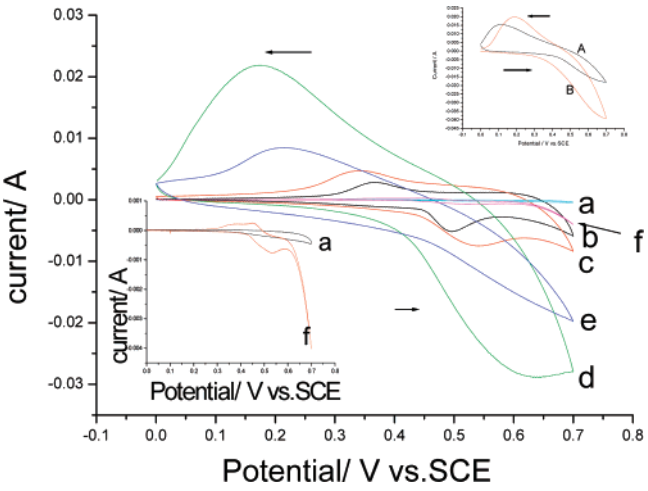

Figure 14. Cyclic voltammograms of the CuNi catalysts and copper foil in an aqueous solution containing 0.1 M NaOH and 1 mM glucose with a scan rate of 50 mV/s. CuNi catalysts were deposited at different potentials, and the electrolysis time was fixed as 600 s. (a) Copper foil, (f) nickel foil, (b−e) CuNi alloy obtained with different potentials: (b) −0.6, (c) −0.8, (d) −1.0, and (e) −1.2 V. CV curves of the CuNi dendritic material electrode in 0.10 M NaOH for the absence (A) and presence (B) of 1.0 mM glucose are shown on the upside. The CuNi dendritic material electrode was obtained at a potential of −1.0 V with an electrolysis time of 600 s. To see the CV curves of (a) copper foil and (f) nickel foil clearly, the inset shows the comparison between the two.

(Figure 11 (2)). At last, the faster one will take the growth space to overwelm the slower one (Figure 11 (4), the white arrow), and the further reduction of Cu^{2+} and Ni^{2+} on the spiral surface possibly results in the elongation of the crystal along the normal direction (Figure 11 (4), the black arrow). With such growth strategies, the 3D growth will come true (Figure 11 (5−7)). (2) The two surfaces will coexist, and two dendrites will be formed with the same root.

To evaluate the CuNi dendritic material electrode as a detector for carbohydrate detection, we studied the electrooxidation ability of glucose in alkaline solution. The deposited CuNi dendritic material electrodes were obtained at different potentials of −0.6, −0.8, −1.0, and −1.2 V (vs SCE) with an electrolysis time of 600 s. As predicted

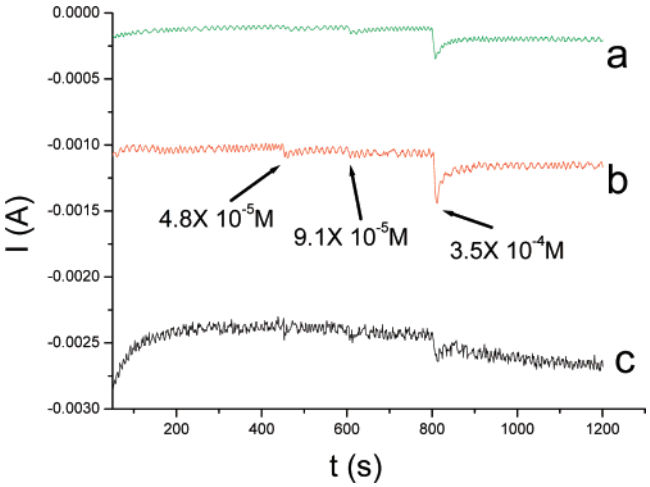

Figure 15. Amperometric responses at pure copper electrode and copper foil electrodes modified by CuNi dendrites as a function of the amount of glucose added at 0.65 V vs SCE. (a) pure copper electrode; (b) CuNi deposit obtained at −0.6 V; (c) CuNi deposit obtained at −1.0 V (vs SCE).

previously, the different potentials applied during the electrolysis will result in the different Cu:Ni ratio compositions and mass deposits, which is shown in Table 4. The more negative the applied potential, the smaller the Cu:Ni elemental ratio will be formed, and more deposits will be obtained. The different Cu:Ni compositions will vary the electrochemical response to the solution in the absence and presence of glucose, which can be exhibited from the cyclic voltammetric curves. More deposits on the surface of the electrode will result in a larger surface area, which will increase the voltammetric response. The curves shown in Figures 13 and 14 are the cyclic voltammetric (CV) responses obtained at the pure Cu, Ni foil, and CuNi dendritic material electrodes in 0.10 M NaOH for the absence and presence of 1.0 mM glucose. From the CV curves shown in Figure 13, the onset potential of O_2 evolution obtained on the CuNi electrode shifts to be more negative than that of the pure copper. This is the evidence that the overpotential is decreased on the surface of the CuNi alloy. The current of O_2 evolution at the alloy surface is much larger than that of the pure copper. Besides the decrease of the overpotential, the high specific surface area is another reason to affect the electrochemical reaction rate. From the voltammetric curves, it is obvious that the different modified electrodes obtained at the different potentials will result in different responses during the electrochemical processes. With the higher Ni composition, the O_2 evolution will be easier to be realized.[46]

For the glucose electrooxidation on the CuNi alloy surface, the relationship between Ni composition and electro-oxidation ability is not monotonous, which is illustrated with the CV responses shown in Figure 14. From Figure 14a−d, with the increase in the Ni in the deposit (the more negative deposition potential is, the larger atomic value of Ni/Cu will be), the oxidation peak current will be increased, but when the electrode modified by CuNi at −1.2 V is applied in the electrooxidation test, its oxidation ability is lower than that of the electrode modified at −1.0 V. For this interesting phenomenon, we assume that the Ni oxidation can easily happen in the Ni-rich dendritic alloy on the surface of the electrode, and the Ni compounds will not be effective for the glucose transformation. For the detailed relationship, it is under our research now.

The Cu foil electrode modified with CuNi dendrites was fabricated as the detector to check the amperometric response to the glucose. Compared with the bare copper electrode, the dendrite-modified electrode obtained at the potential of −0.6 V is more sensitive to the glucose. Shown in Figure 15, the response can be distinguished when the glucose concentration reaches at least 4.8×10^{-5} M. Research is being conducted on the detailed relationship among CuNi composition, electrolysis time, deposition potential, and the sensitivity to glucose and other organic compounds.

Conclusions

In conclusion, CuNi dendritic material has been obtained by the chronoamperometry technique. Different potentials were applied to get the dendritic structure from the mixed solution containing Cu^{2+} and Ni^{2+}. The materials were characterized by a series of techniques to show the dendritic morphology and crystal structure. The dendritic morphology formations are discussed from the aspects of thermodynamics and kinetics to give a deep understanding of the crystal growth. For the practical application of the material in fuel cells and biosensors, we tested the electro-oxidation ability of glucose.

Acknowledgment. This work was supported by Korean Research Foundation Program. Special thanks are given to the financial support of Brain Korea 21.

CM070638A

(46) Yeo, I. H.; Johnson, D. C. *J. Electroanal. Chem.* **2001**, *495*, 110.